Transient arousal modulations are responsible for resting-state functional connectivity changes associated with head motion

Yameng Gu[1], Feng Han[1], Lucas E. Sainburg[1], Xiao Liu[1,2]*

[1]Department of Biomedical Engineering, The Pennsylvania State University, PA, USA;

[2]Institute for CyberScience, The Pennsylvania State University, PA, USA;

* Corresponding Author: Xiao Liu, PhD

315 Hallowell Building

The Pennsylvania State University

University Park, PA 16802-4400

Tel: +1 814 863 4419

E-mail: xxl213@engr.psu.edu

Keywords: resting-state fMRI; functional connectivity; head motion; global signal; arousal modulations.

Abstract

Correlations of resting-state functional magnetic resonance imaging (rsfMRI) signals are being widely used for assessing functional connectivity of healthy and diseased brains. However, an association was recently observed between rsfMRI connectivity modulations and head motion and regarded as a causal relationship, which has raised serious concerns about the validity of many rsfMRI findings. Here, we studied the origin of this rsfMRI-motion association and its relationship to arousal modulations. By using a template-matching method to locate arousal-related fMRI changes, we showed that the effects of high motion time points on rsfMRI connectivity are due to their significant overlap with arousal-affected time points. The finding suggests that the association between rsfMRI connectivity and head motion arises from their co-modulations at transient arousal modulations, and this information is critical not only for proper interpretation of motion-associated rsfMRI connectivity changes but also for controlling the potential confounding effects of arousal modulation on rsMRI metrics.

Introduction

Resting-state functional magnetic resonance imaging (rsfMRI) signal correlations have been widely used to assess functional brain connectivity and greatly improved our understanding of intrinsic organization of healthy and diseased brains (1–3). However, the validity of a large body of rsfMRI studies was recently challenged by findings about the relationship between head motion and rsfMRI connectivity (4–7). Subjects associated with larger head motions during scanning were found to show significantly stronger local rsfMRI connectivity and weaker long-range connectivity (6). Consist with this relationship, scrubbing rsfMRI time frames with severe head motion successfully reduced local and recovered long-range brain connectivity (7). More recently, the head motion was further suggested to mediate the correlation between the rsfMRI connectivity and behavioral measurements (8). To date, the observed motion-connectivity relationship has been interpreted as a causal relationship with the assumption that the head motion corrupts rsfMRI data and thus functional connectivity derived from it. The relationship is also regarded as a piece of evidence for non-neuronal contributions to the rsfMRI connectivity.

However, the neuronal contribution to this motion-connectivity relationship cannot be completely ruled out. A major motion metric, i.e., differentiated signal variance (DVARS) (9), measures large fMRI signal modulations that are not necessarily caused by the motion, and it often detects brain-wide, synchronized fMRI changes (often called the “global signal”), which have been consistently linked to low vigilance brain states (10–16) and appear to be at least partly neuronal (17). This global fMRI signal was recently found to arise from global brain co-activations that are induced by an event of transient arousal modulation with a characteristic electrophysiological signature (18). This finding, along with the known association between head motion and sleepiness (19), suggests a possibility that the transient arousal modulations cause both head motion and rsfMRI connectivity changes and thus a spurious relationship between the two. The validity of this hypothesis would reconcile a few puzzling observations about the motion-connectivity relationship. For example, the specific sensory-dominant pattern of the arousal-related global co-activations (18) may explain systematic and divergent changes in local and long-range rsfMRI connectivity associated with head motion. The hemodynamic delay of neurovascular coupling may account for the long-lasting (more than 10 seconds) effects of motion on the rsfMRI connectivity (4, 20). It may also provide a new perspective for understanding the observation that the same amount of head motion causes significant rsfMRI connectivity changes across subjects but not different sessions from the same subject (21).

A clear understanding of the origin of the motion-connectivity relationship is critical for a proper interpretation of findings from a large body of rsfMRI studies. Towards this goal, we use the Human Connectome Project (HCP) data (22) to examine the role of transient arousal modulations in mediating the association between head motion and rsfMRI connectivity changes. Utilizing a template of the global co-activation pattern induced by a transient arousal event (18), we derived a drowsiness index to locate arousal-related rsfMRI changes. We then demonstrated that the effect of motion-based temporal scrubbing on rsfMRI connectivity should be attributed to arousal-related rsfMRI changes. We further understand this result by elucidating a rather complicated temporal relationship between the motion and arousal metrics through a trial-based analysis. Finally, we demonstrated, with simulation, how the arousal-related fMRI co-activations can cause systematic modulations in whole-brain rsfMRI connectivity similar to those associated

with head motions. Overall, the results suggest that the association between head motion and rsfMRI connectivity is not causal but mediated by transient arousal modulations.

Results

We analyzed HCP rsfMRI data of 469 subjects who completed all four resting-state sessions in two different days. Four indices were derived from the rsfMRI signals. Framewise displacement (FD) (23) and DVARS (9) have both been used for assessing head motion, but they may present different information since the former is derived directly from image alignment parameters whereas the latter quantifies the amplitude of fMRI changes between consecutive time points. Since the global rsfMRI signal has been consistently shown to be sensitive to brain vigilance states (10–16), we take its envelop amplitude (GSA) as an approximate estimate for instantaneous arousal level. It was shown recently that the large global rsfMRI peak originates from a global fMRI co-activation that is induced by a transient arousal event and shows a sensory-dominant pattern (18). To incorporate this spatial information, we adapt the idea of a template-matching approach (24), correlate this global co-activation pattern with individual rsfMRI volumes, and then take the envelop amplitude as an index to estimate arousal fluctuations (Fig. 1). Because the large global co-activation and the associated electrophysiological event appear mostly at intermediate states of vigilance (18), such as drowsy state and light sleep, we name the fourth metric as the drowsiness index (DI) (See Methods for details about how to derive these four metrics).

Motion and arousal metrics are related to arousal

All four metrics showed a tendency of increasing amplitude over the course of rsfMRI scanning. This effect was much stronger for the arousal indices, i.e., the GSA and DI, but also present for the motion metrics, i.e., the FD and DVARS (Fig. 2*A*). This temporal trend likely indicates an increasing probability for subjects becoming drowsy or falling asleep, which is consistent with a previous finding that a significant proportion of subjects fell asleep within 3 minutes into the resting-state scanning (25).

In addition to the intra-subject trend, we also examined the relationship between these metrics and arousal-related behavioral measures across subjects. Towards this goal, we correlated the individual's DI score, defined as the mean DI averaged over all 4 sessions, with the Pittsburgh Sleep Questionnaire (PSQ) items provided along with fMRI data by the HCP. FD and DI are significantly correlated with multiple PSQ items. The items correlated with DI appear to be related to the sleep propensity of subjects. The subjects who go to bed later ($p = 9.4\text{x}10^{-4}$) and have less amount of sleep ($p = 0.027$) showed significantly higher DI scores. In contrast, FD is significantly correlated with the items reflecting the comfort in sleeping position. The subjects who reported to snore ($p = 3\text{x}10^{-5}$), cannot breathe comfortably ($p = 0.0070$), or felt too hot ($p = 0.027$) during sleep are associated with significantly higher FD values (Fig. 2*B* and Table 1). In addition, the individual DI score is also found significantly higher in a group of subjects who were noted to be sleeping during the resting-state fMRI scanning (Fig. 2*C*). Overall, both the intra- and inter-subject analyses suggest a close relationship between those motion and arousal metrics, particularly DI, and brain arousal levels.

Temporal scrubbing effects on rsfMRI connectivity based on different metrics

Scrubbing time points with a high value in motion metrics has become a commonly used approach to alleviate the influence of the motion on rsfMRI connectivity (4, 7). Here we

compared the effects of temporal scrubbing on rsfMRI connectivity based on the four metrics. We assessed the whole-brain rsfMRI connectivity using Pearson's correlation coefficients between fMRI time courses of each possible pair of 264 regions of interest (ROIs) (26), then estimated temporal scrubbing effects using the connectivity difference before and after scrubbing time points with the top 25% values in a specific metric.

Consistent with the previous findings (4–7), the temporal scrubbing based on FD and DVARS decreased local but increased long-range rsfMRI connectivity (Fig. 3*A* and 3*B*). Nevertheless, the scrubbing based on FD, which were computed directly from image alignment parameters (23), showed a much smaller effect than the DVARS-based scrubbing. This could be due to the fact that DVARS (9) is, by definition, sensitive to large fMRI changes that are not necessarily caused by the head motion. Scrubbing time points of high GSA values produced a similar level of effect on the rsMRI connectivity as the DVARS-based scrubbing (Fig. 3*C*). The largest changes in local and long-range rsfMRI connectivity were observed with excluding the top 25% DI time points (Fig. 3*D*). Therefore, the arousal-related fMRI changes, flagged by high DI values, affect rsfMRI connectivity in a similar way as head motion does but to a much larger extent.

We then examined metric-specific scrubbing effects since significant overlaps are expected between scrubbed time points based on different metrics. Indeed, 39% of scrubbed, i.e., 9.81% of the total, time points are the same for the DVARS- and DI-based scrubbing, and this value is significantly higher ($p = 0$; permutation test, $n = 10{,}000$) than the one (6.25% of the total) expected if these two metrics are completely independent. After excluding these overlapped time points from scrubbing, i.e., retaining them for rsfMRI connectivity assessments, the DVARS-specific scrubbing produced no significant changes on either local or long-range rsfMRI connectivity, but the effect of DI-specific scrubbing remained large (Fig. 4). A similar result was obtained for the pair of FD and DI (Fig. S1). The finding clearly suggests that the effect of motion-based scrubbing on rsMRI connectivity should be entirely attributed to time points of high DI values, which are closely related to arousal modulations.

Temporal relationship between the motion and arousal metrics

A clear understanding of the above findings would require details about the temporal relationship between the motion and arousal metrics. Cross-correlation functions calculated between all possible pairs of FD, DVARS, and DI revealed a rather complicated temporal relationship among them. The cross-correlation function between DI and DVARS had a single peak at the zero delay (Fig. 5*A*, left**)**, whereas FD and DI reached their maximum correlation with DI being shifted ahead by about 9 seconds (Fig. 5*A*, middle**)**. More interestingly, the cross-correlation function for the FD-DVARS pair showed two separate peaks with one at the zero delay and the other with a significant delay (Fig. 5*A*, right**)**. The peak correlation between FD and DI is smaller than those of the other two pairs.

To understand this complex relationship, we employed a trial-based analysis to examine the relative timing of large changes in different metrics, as well as the variability of this relationship over time. The feasibility of this analysis lies in the observation that FD often shows large, abrupt spikes that appear to drive its correlation with DVARS and DI (Fig. S2). We identified 3331 FD spikes by finding FD peak points that are 3 standard deviations above the mean. Removing these spikes (4.2 % of the total points) would bring down the covariance between FD

and DVARS by 79 % (from 0.0169 to 0.0036). We then extracted FD, DVARS, and DI segments centering on the FD spikes and sorted these segments according to DI values at 9.36 seconds, where we expected to see large peaks according the FD-DI correlation function (Fig. 5*A*, middle). We found that a subset of the FD spikes is followed by a DI peak delayed by ~9 second, and they correspond to two separate DVARS peaks (Fig. 5*B*, bottom trials). In comparison, there are also FD spikes that are associated with only a zero-lag DVARS peak (Fig. 5*B*, top trials). We also displayed the DVARS scrubbing mask (Fig. 5*C*, right), as well as its overlap with (Fig. 5*C*, middle) and difference from (Fig. 5*C*, left) the DI scrubbing mask for all these trials. As expected, the overlap between the DVARS and DI masks, which is responsible for the scrubbing effect on rsfMRI connectivity (Fig. 4), corresponds mostly to the delayed DI/DVARS peaks following the FD spikes (Fig. 5*C*, middle). In other words, the head motions that are not followed by arousal-related fMRI changes, i.e., the large DI peaks, are not associated with significant changes in rsfMRI connectivity (top trials in Fig. 5*B* and 5*C*). The above analysis was repeated with replacing DI with GSA, as well as the GSA calculated with excluding the entire sensorimotor cortex, and the major results remained the same (Fig. S3). Thus, it is unlikely that the DI peaks following the FD spikes are caused by sensorimotor activations responsible for the head motion. Instead, the FD spikes and delayed DI peaks in a subset of trials likely originate from transient arousal modulations, and their relative delay may reflect, at least partly, the hemodynamic delay between neural/behavioral signals and fMRI.

Arousal-related global co-activation and systematic rsfMRI connectivity changes

The motion-related rsfMRI connectivity changes have been found to show systematic patterns, including the opposite modulations in local and long-range connectivity (5–7). We have shown so far that the motion-associated rsfMRI connectivity changes are actually caused by the high DI time points with a global co-activation pattern of arousal relevance. Although the sensory-dominant pattern of this global co-activation (Fig. 1*A*) is expected to promote local connectivity in sensory areas, it is much harder to understand intuitively how this co-activation pattern may reduce long-range rsfMRI connectivity especially given the global signal regression procedure. To address this issue, we simulated chunks of fMRI signals with this global co-activation pattern, inserted them into real rsfMRI data, and then examined rsfMRI changes caused by removing them. Scrubbing these simulated chunks of data with the global co-activation pattern indeed reduced the local but increased the long-range rsfMRI connectivity, similar to the DVARS-based temporal scrubbing (Fig. 6*A*). Expanding these 1D profiles of distance dependency to 2D matrices of inter-regional connections revealed that the reduced connectivity resided mostly within the sensory regions as expected whereas the increased connections were largely across brain networks, which resembled the effect of DVARS-based scrubbing (r = 0.38, p = 0, Fig. 6*B* and 6*C*). This simulation clearly showed how the arousal-related rsfMRI modulations, i.e., the global co-activation with a sensory-dominant pattern, can result in systemic rsfMRI connectivity changes.

Discussion

Here we showed that the association between head motion and rsfMRI connectivity, which has been interpreted as a causal relationship (4–7), may arise spuriously from transient arousal modulations. We first developed an fMRI-based arousal index, i.e., DI, to track arousal modulations and validated this index through its correlations with arousal-related behavioral measures. We then showed that the effect of temporal scrubbing based on the motion parameters,

i.e., FD and DVARS, on rsfMRI connectivity is actually attributed to time points associated with transient arousal modulations. We further elucidated complex temporal relationships among the motion and arousal indices using a trial-based analysis, and the relationship between rsfMRI connectivity and the global co-activation pattern of arousal relevance using simulation.

The association between head motion and rsfMRI connectivity can be linked to arousal modulations in two ways. First, a significant proportion of this relationship comes spuriously from the use of DVARS, a widely used index for quantifying head motion based on fMRI signal itself. The DVARS index is defined as the root mean square of whole brain fMRI signal changes between consecutive time points and thus sensitive to any large, widespread fMRI changes. Although it was designed to detect head motion (9), it should be also sensitive to transient arousal modulations, which have been shown to induce large, global fMRI changes (10–16). The two DVARS peaks that correspond to the FD spike and following DI peak in our trial-based analysis (Fig. 5*B*, bottom trials) likely represent these two types of DVARS modulations. On the other hand, the observed coupling between the FD spikes and DI peaks, though with a significant time delay, could be the second source of the motion-rsfMRI relationship and account for the marginal scrubbing effect based on FD, which is derived from image alignment parameters and thus closely related to real head motions. The sleepiness induced by sleep deprivation has been found to be associated with more head motions compared with wakefulness (19). Similar to the coupling between the FD and DI peaks, this could be caused by transient arousal modulations and associated physiological changes during the drowsy and sleepy states. It is also worth noting that the DI/GSA peak following the FD spike should not be attributed to head motion related sensorimotor activity and associated fMRI changes since removing the entire sensorimotor cortex from the GSA calculation had almost no effects on the result (Fig. S3).

The role of arousal modulations in causing the spurious motion-rsfMRI relationship explains a few puzzling observations. First, the effect of head motion on rsfMRI connectivity persists for, and even reach its peak at, more than 10 seconds (4, 20). Although this observation has been explained from the perspective of spin-history artifacts (27), this explanation may not be satisfactory because the spin-history artifact induced by a brief motion should not last for so long and show its peak effect after 10 seconds (20). This prolonged effect is even longer than the typical hemodynamic delay between neural and fMRI signals. However, this characteristic time is roughly consistent with the delay we observed here between FD spikes and DI peaks. The co-occurrence of FD spikes and large fMRI changes (the large DI/GSA) could be mediated by transient arousal events, and their relative time delay may include both the hemodynamic delay and their relative phases in the arousal event. Second, the motion-related rsfMRI connectivity changes are not only distance dependent but also show very systematic spatial patterns (7). Although this is hard to understand from the perspective of head motion, which is relatively random, it is consistent with the sensory-dominant fMRI co-activations associated with arousal modulations. We indeed confirmed, with simulation, that the arousal-related fMRI changes, i.e., the global fMRI co-activation pattern, modulates the similar set of rsfMRI connections as the motion-based scrubbing procedure.

Transient arousal modulations may also mediate the correlations between rsfMRI signals and other measurements in a similar way. Strong correlations have been found between rsfMRI signal/connectivity and physiological signals, e.g., the heart rate and respiratory volume, which

was also regarded as evidence for non-neuronal contributions to rsfMRI (28–30). However, the rsfMRI-physiology correlation was recently found significant only under a sleep-conducive eyes-closed condition but not under a more alert eyes-open condition (29). This correlation was also dependent on the EEG alpha power, an indicator of brain vigilance state (29).Therefore, it is likely that the rsfMRI-physiological correlation may arise from the effects of transient arousal modulations on both autonomic functions and fMRI signals. This hypothesis is consistent with the observation that the FD motion is not only followed by the global fMRI signal change but also co-varies with respiratory modulations (20). In fact, the respiratory modulations, e.g., a deep breath, at transient arousal modulations might be the direct cause of head motion and account for increased head motion under the sleepy condition (19). Similarly, one should be cautious about the confounding effects of arousal in rsfMRI studies of various brain diseases, a significant portion of which are either associated with disrupted sleep and circadian rhythms or treated with medicines that can modulate brain arousal state (31–35). Thus, it is important to differentiate rsfMRI changes caused by disease-related brain reorganization from those merely reflecting disease-associated vigilance changes. Arousal may affect cognitive performance given its known role in attention regulation and information processing (36), and the ability of regulating arousal state may also be correlated with other subject traits (37). Therefore, transient arousal modulations might be partly responsible for the correlation observed between rsfMRI connectivity/dynamics and behavioral measures (38–40). Given these potential confounding effects of the arousal, researchers should be cautious about large global fMRI signals, high DI values, and the sensory-dominant pattern in their rsfMRI findings, which are all indicators of arousal-related fMRI changes.

Properly controlling the effects of arousal modulations on rsfMRI signals is critical for unraveling real changes in functional brain connectivity. Prospective studies need to better control and monitor arousal fluctuations during resting-state scans, which can be achieved by, for example, avoiding rsfMRI experiments under sleep-conducive eyes-closed condition and/or including EEG or eyelid video with fMRI acquisitions. Retrospective analyses on existing datasets should try to minimize the arousal's influence with appropriate post-processing procedures. Although the global signal regression can largely suppress the arousal-related component, the residual effect on rsfMRI connectivity is clearly present (Fig. 6). Given that the arousal modulations take the form of transient events that are temporally separable, removing arousal-contaminated time points from the analysis could be a way of reducing the arousal's influence. The DI used in this study and other fMRI-based arousal indices (24, 41) are preferred metrics for such temporal censoring procedures and expected to locate arousal-related fMRI changes more accurately than the motion parameters. However, even assuming the temporal censoring can effectively remove the direct effect of the transient arousal modulations, it is unclear whether the brain connectivity/dynamics are modulated even outside of the time periods of those arousal events under drowsy and sleepy conditions. A more conservative way of controlling the arousal's effect would be to completely discard sessions/subjects showing large arousal modulations, which can be assessed again according to the fMRI-based arousal indices, such as DI, if no external arousal measure available. Alternatively, this could be done by including individuals' arousal score as a nuisance variable into the statistical model that compares rsfMRI metrics under different groups or brain conditions.

The DI, an fMRI-based arousal index, was used to locate arousal-related fMRI changes. It was derived by correlating individual fMRI volumes with the global co-activation pattern that has been shown to be induced by an electrophysiological event of transient arousal modulation (18). The similar template-matching methods were used for arousal estimation with different templates, including the fMRI correlation maps of the EEG arousal index or behavioral arousal index defined by eyelid positions (24, 41). These different templates show very similar sensory-dominant patterns and may thus originate from the same event of arousal modulations (18). These fMRI-based arousal indices can capture the intra-subject dynamics and the inter-subject variability of arousal modulations. These indices can provide a flexible and convenient estimate of the brain arousal level to any data sets with rsfMRI data, including recent large-scale imaging initiatives collected from healthy subjects and patients, e.g., the UK Biobank (42) and Alzheimer's Disease Neuroimaging Initiative (ADNI) (43). Along with other imaging and behavioral data, this may create new opportunities to understand arousal regulation mechanisms as well as the arousal's role in neurological diseases showing abnormal arousal regulations, e.g., Alzheimer's disease (44, 45).

In summary, the rsfMRI connectivity changes associated with head motion are not caused by the motion itself but by transient arousal modulations, which have been shown to induce profound fMRI changes. The arousal-related fMRI change may potentially confound the relationships between rsfMRI connectivity and other measures. Caution should be exercised if large global rsfMRI signals, higher values in fMRI-based arousal indices, or sensory-dominant brain maps is found in rsfMRI analyses.

Methods

HCP data

The human connectome project (HCP) 500-subject data release was used. The HCP 500-subject data release included 526 subjects who were scanned on a 3T Siemens Skyra scanner. We limited our analyses to 469 subjects (age: 29.2 ± 3.5 years, 275 females) who completed all four rsfMRI sessions. Each subject contributed four 15-min sessions on two separate days (two sessions per day). The data were acquired with multiband echo-planar imaging with a temporal resolution of 0.72 sec and spatial resolution of 2-mm isotropic voxels.

The HCP MR minimal preprocessing pipelines were applied. MR functional pipelines applied to the fMRI data included the following steps: distortion correction, motion correction, registration to structural data, and conversion to gray-ordinates standard space. Next, the resting state fMRI data were run over the HCP FIX-ICA denoising pipeline to remove artifacts. In addition to the minimal preprocessing pipelines, we smoothed the data temporally (0.001-0.1 Hz) and further standardized each voxel's signal by subtracting the mean and dividing the standard deviation.

Framewise displacement (FD)

Framewise displacement (FD) was estimated using a method described previously (23). Specifically, FD was calculated as the sum of absolute values of six differentiated head realignment parameters at each frame as follows:

$$FD_i = |\Delta d_{ix}| + |\Delta d_{iy}| + |\Delta d_{iz}| + |\Delta \alpha_i| + |\Delta \beta_i| + |\Delta \gamma_i|$$

where $[d_{ix}\ d_{iy}\ d_{iz}]$ are three translational parameters and $[\alpha_i\ \beta_i\ \gamma_i]$ are three rotational parameters. $|\Delta d_{ix}| = |d_{(i-1)x} - d_{ix}|$ and the other parameters were calculated in the same way. The three rotational parameters were calculated as the displacement of millimeters converted from degrees on the sphere surface with a radius 50 mm, which was the approximate average distance from the cerebral cortex to the center of the human head.

DVARS

DVARS is defined as the rate of fMRI signal changes over the entire brain at each frame (9). Global signal regression was applied on the HCP minimal rsfMRI preprocessed data before calculating DVARS. DVARS is calculated as the root mean square value within the whole brain of differentiated fMRI time courses at each frame:

$$DVARS(\Delta I)_i = \sqrt{\langle[\Delta I_i(\vec{x})]^2\rangle} = \sqrt{\langle[I_i(\vec{x}) - I_{i-1}(\vec{x})]^2\rangle}$$

where $I_i(\vec{x})$ is the image intensity at locus x at the ith frame and the angle brackets indicate the spatial average from the whole brain.

Global signal amplitude (GSA) and drowsiness index (DI)

Global signal was calculated as the mean signal averaged over all gray matter voxels, and the global signal amplitude (GSA) is then defined as the envelop amplitude of the global signal. Adapting a template-matching strategy (24), the spatial correlation between the global co-activation pattern and rsfMRI volumes at individual time points was calculated and its envelop amplitude was defined as the drowsiness index (DI).

ROIs

All fMRI time courses used in this study were extracted from a set of 264 regions of interest (ROIs), which are spheres of 10 mm diameter centered on the coordinates given by a previous study (26). The rsfMRI correlations among the 264 ROIs were calculated after the global signal regression procedure.

Relating arousal-related behavioral measures to the motion and arousal metrics

Among a total of 295 behavioral, demographic, and physiological measures released with the HCP data set, we selected and correlated 20 items from the Pittsburgh Sleep Questionnaire (PSQ) with mean FD, DVARS, GSA and DI averaged over four sessions of each subject. Bed times after midnight were treated as the original bed times plus 24 hours.

Temporal scrubbing procedure

The first and last 20 time points from FD, DVARS, GSA and DI time courses were removed from the subsequent analyses since they showed an abnormal pattern that likely resulted from the ICA-FIX procedure. Temporal masks were generated to mark the 25% time points of all the subjects showing the highest values in FD, DVARS, GSA, and DI, respectively. A control mask was also created by circularly shifting the FD mask by 600 time points. In addition, the DVARS-specific and DI-specific masks were generated by excluding their overlapped part. Temporal scrubbing was performed with respect to different masks. RsfMRI correlations of the 264 pre-defined ROIs were computed for scrubbed (r') and unscrubbed (r) data for each subject. Their difference ($\Delta r = r' - r$) was calculated and then averaged across subjects. The differences (Δr) were plotted as a function of Euclidean distance between the ROIs. The rsfMRI connectivity changes for ROI pairs with a Euclidean distance of 13 ~ 49 mm and of 125 ~ 161 mm were

averaged to represent local and long-range connectivity changes respectively. Similar results were obtained for the pair of FD-based and DI-based masks.

Temporal relationship among FD, DVARS and DI

Cross-correlation functions between each pair of FD, DVARS and DI were calculated. The mean of FD, DVARS, and DI time courses were removed to reduce inter-subject variation in the baselines. FD spikes were located by finding peaks exceeding 3 standard deviations above the mean within each FD time course. Segments of the FD, DVARS, and DI time courses centering on the FD spikes (±28.8 seconds) were extracted respectively. Segments of FD, DVARS, and DI were sorted according to the DI values at 9.36 second, where a proportion of DI segments show consistent peaks. After sorting, the first and last 400 segments were averaged and their difference was also calculated. GSA segments were calculated and processed in the same way with and without excluding the sensorimotor regions. The corresponding segments of the DVARS-based mask as well as its overlap with and difference from the DI-based mask were extracted and processed.

Simulation

The simulation was used to understand the systematic changes in rsfMRI connectivity caused by the global fMRI co-activation pattern of arousal relevance. The template of the global co-activation pattern was convolved with the canonical hemodynamic response function to generate chunks of simulated rsfMRI data with each containing 46 brain volumes. The fluctuation amplitude of simulated data was scaled to match with that of the real data. Eight chunks were randomly inserted into the real rsfMRI data of the 100 subjects with the lowest DI scores. The template of the global co-activation pattern was convolved by canonical hemodynamic response function to generate chunks of simulated rsfMRI data, which were then inserted into the rsfMRI data of the 100 subjects who show lowest DI scores. The rsfMRI data containing the simulated chunks went through the global signal regression procedure. The pair-wise correlations between the 264 ROIs were then calculated before and after removing the simulated portion, and their differences were regarded as the rsfMRI connectivity changes caused by the global co-activation pattern that has been shown to be induced by an event of transient arousal modulation (18). The 264 ROIs were classified into different brain networks using a brain atlas from (26).

Acknowledgements

This research was supported by the NIH Pathway to Independence Award (K99/R00) 4R00NS092996-02. We thank Matthew F. Glasser for sharing the information about subjects' sleeping state inside the scanner.

Contributions

Y.G. and X.L. designed the study and performed the analyses; Y.G., X.L., F.H., and L.S. wrote the paper.

Competing financial interests

The authors declare no competing financial interests.

References

1. Fox MD, Raichle ME (2007) Spontaneous fluctuations in brain activity observed with functional magnetic resonance imaging. *Nat Rev Neurosci* 8(9):700–711.
2. Biswal B, FZ Y, VM H, JS H (1995) - Functional connectivity in the motor cortex of resting human brain using echo-planar MRI. *Magn Reson Med* 34(9):537–541.
3. Zhang D, Raichle ME (2010) Disease and the brain's dark energy. *Nat Rev Neurol* 6(1):15–28.
4. Power JD, et al. (2014) Methods to detect, characterize, and remove motion artifact in resting state fMRI. *Neuroimage* 84:320–341.
5. Satterthwaite TD, et al. (2012) Impact of in-scanner head motion on multiple measures of functional connectivity: Relevance for studies of neurodevelopment in youth. *Neuroimage* 60(1):623–632.
6. van Dijk KRA, Sabuncu MR, Buckner RL (2012) The influence of head motion on intrinsic functional connectivity MRI. *Neuroimage* 59(1):431–438.
7. Power JD, Barnes KA, Snyder AZ, Schlaggar BL, Petersen SE (2012) Spurious but systematic correlations in functional connectivity MRI networks arise from subject motion. *Neuroimage* 59(3):2142–2154.
8. Siegel JS, et al. (2017) Data quality influences observed links between functional connectivity and behavior. *Cereb Cortex* 27(9):4492–4502.
9. Smyser CD, et al. (2010) Longitudinal analysis of neural network development in preterm infants. *Cereb Cortex* 20(12):2852–2862.
10. Wong CW, Olafsson V, Tal O, Liu TT (2013) The amplitude of the resting-state fMRI global signal is related to EEG vigilance measures. *Neuroimage* 83:983–990.
11. Licata SC, et al. (2013) The hypnotic zolpidem increases the synchrony of BOLD signal fluctuations in widespread brain networks during a resting paradigm. *Neuroimage* 70:211–222.
12. Kiviniemi VJ, et al. (2005) Midazolam sedation increases fluctuation and synchrony of the resting brain BOLD signal. *Magn Reson Imaging* 23(4):531–537.
13. Greicius MD, et al. (2008) Persistent default-mode network connectivity during light sedation. *Hum Brain Mapp* 29(7):839–847.
14. Fukunaga M, et al. (2006) Large-amplitude, spatially correlated fluctuations in BOLD fMRI signals during extended rest and early sleep stages. *Magn Reson Imaging* 24(8):979–992.
15. Wong CW, DeYoung PN, Liu TT (2016) Differences in the resting-state fMRI global signal amplitude between the eyes open and eyes closed states are related to changes in EEG vigilance. *Neuroimage* 124:24–31.
16. He H, Liu TT (2012) A geometric view of global signal confounds in resting-state functional MRI. *Neuroimage* 59(3):2339–2348.
17. Scholvinck ML, Maier A, Ye FQ, Duyn JH, Leopold DA (2010) Neural basis of global resting-state fMRI activity. *Proc Natl Acad Sci* 107(22):10238–10243.
18. Liu X, et al. (2018) Subcortical evidence for a contribution of arousal to fMRI studies of brain activity. *Nat Commun* 9(1):1–10.
19. VAN DEN BERG J (2006) Sleepiness and Head Movements. *Ind Health* 44(4):564–576.
20. Byrge L, Kennedy DP (2018) Identifying and characterizing systematic temporally-lagged BOLD artifacts. *Neuroimage* 171(December 2017):376–392.

21. Zeng L-L, et al. (2014) Neurobiological basis of head motion in brain imaging. *Proc Natl Acad Sci* 111(16):6058–6062.
22. Van Essen DC, et al. (2013) The WU-Minn Human Connectome Project: An overview. *Neuroimage* 80:62–79.
23. Yoo SS, Choi BG, Juh R, Pae CU, Lee CU (2005) Head motion analysis during cognitive fMRI examination: Application in patients with schizophrenia. *Neurosci Res* 53(1):84–90.
24. Chang C, et al. (2016) Tracking brain arousal fluctuations with fMRI. *Proc Natl Acad Sci* 113(16):4518–4523.
25. Tagliazucchi E, Laufs H (2014) Decoding Wakefulness Levels from Typical fMRI Resting-State Data Reveals Reliable Drifts between Wakefulness and Sleep. *Neuron* 82(3):695–708.
26. Power JD, et al. (2011) Functional Network Organization of the Human Brain. *Neuron* 72(4):665–678.
27. Yancey SE, et al. (2011) Spin-history artifact during functional MRI: Potential for adaptive correction. *Med Phys* 38(8):4634–4646.
28. Birn RM, Diamond JB, Smith MA, Bandettini PA (2006) Separating respiratory-variation-related fluctuations from neuronal-activity-related fluctuations in fMRI. *Neuroimage* 31(4):1536–1548.
29. Yuan H, Zotev V, Phillips R, Bodurka J (2013) Correlated slow fluctuations in respiration, EEG, and BOLD fMRI. *Neuroimage* 79:81–93.
30. Chang C, et al. (2013) Association between heart rate variability and fluctuations in resting-state functional connectivity. *Neuroimage* 68:93–104.
31. Breen DP, et al. (2014) Sleep and circadian rhythm regulation in early parkinson disease. *JAMA Neurol* 71(5):589–595.
32. Cohen S, Conduit R, Lockley SW, Rajaratnam SMW, Cornish KM (2014) The relationship between sleep and behavior in autism spectrum disorder (ASD): a review. 6(1):1–10.
33. Whitfield-Gabrieli S, et al. (2009) Hyperactivity and hyperconnectivity of the default network in schizophrenia and in first-degree relatives of persons with schizophrenia. *Proc Natl Acad Sci* 106(4):1279–1284.
34. Musiek ES, Xiong DD, Holtzman DM (2015) Sleep, circadian rhythms, and the pathogenesis of Alzheimer disease. *Exp Mol Med* 47(3):e148.
35. Yang GJ, et al. (2014) Altered global brain signal in schizophrenia. *Proc Natl Acad Sci* 111(20):7438–7443.
36. Pribram KH, McGuiness D (1975) Arousal, activatio, and effort in the control of attention. *Psychol Rev* 82(2):116–149.
37. Lagarde D, Batejat D (1994) Evaluation of drowsiness during prolonged sleep deprivation. *Neurophysiol Clin / Clin Neurophysiol* 24(1):35–44.
38. Liu X, Duyn JH (2013) Time-varying functional network information extracted from brief instances of spontaneous brain activity. *Proc Natl Acad Sci* 110(11):4392–4397.
39. Chang C, Glover GH (2010) Time-frequency dynamics of resting-state brain connectivity measured with fMRI. *Neuroimage* 50(1):81–98.
40. Gui D, et al. (2015) Resting spontaneous activity in the default mode network predicts performance decline during prolonged attention workload. *Neuroimage* 120:323–330.
41. Falahpour M, Chang C, Wong CW, Liu TT (2018) Template-based prediction of vigilance fluctuations in resting-state fMRI. *Neuroimage* 174(January):317–327.

42. Miller KL, et al. (2016) Multimodal population brain imaging in the UK Biobank prospective epidemiological study. *Nat Neurosci* 19(11):1523–1536.
43. Jack CR, et al. (2008) The Alzheimer's Disease Neuroimaging Initiative (ADNI): MRI methods. *J Magn Reson Imaging* 27(4):685–691.
44. Musiek ES, et al. (2018) Circadian rest-activity pattern changes in aging and preclinical Alzheimer disease. *JAMA Neurol* 75(5):582–590.
45. Carvalho DZ, et al. (2018) Association of excessive daytime sleepiness with longitudinal β-Amyloid accumulation in elderly persons without dementia. *JAMA Neurol* 75(6):672–680.

Figures

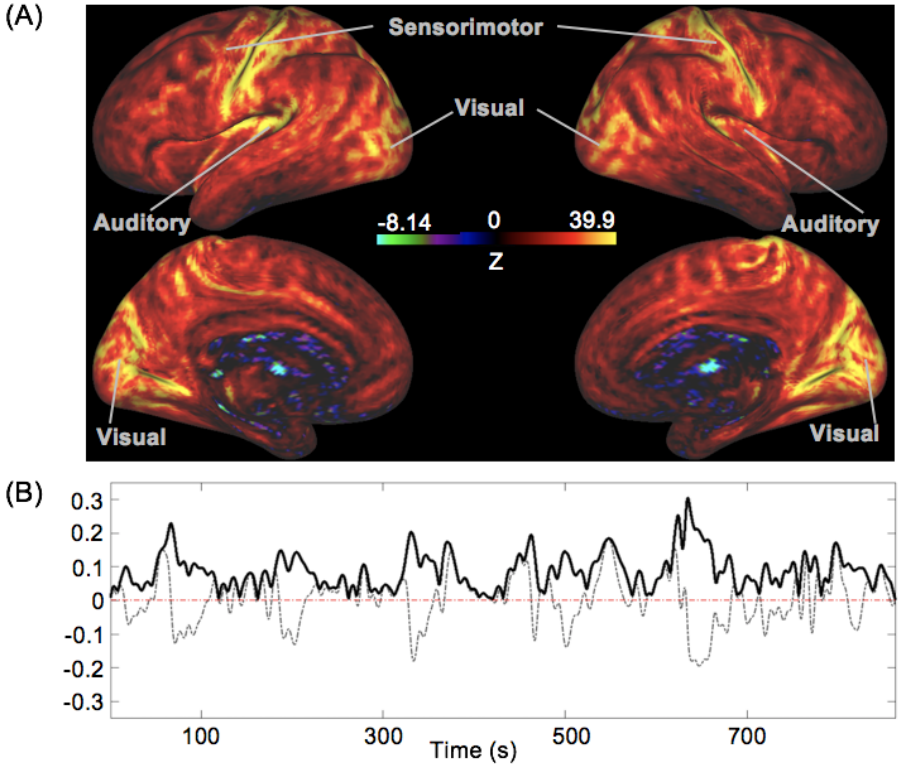

Figure 1 Drowsiness index (DI) derived in a representative subject. (A) The global fMRI co-activation pattern, which has been shown to be induced by an event of transient arousal modulation, is used as a template for deriving DI. Sensorimotor, visual, and auditory regions show larger signal increase than other cortical regions and some subcortical areas show signal decreases. (B) An example of the DI time course of a representative subject. DI is defined as the envelop amplitude (solid black) of the spatial correlations (dashed gray) between the global co-activation pattern (A) and individual fMRI volumes.

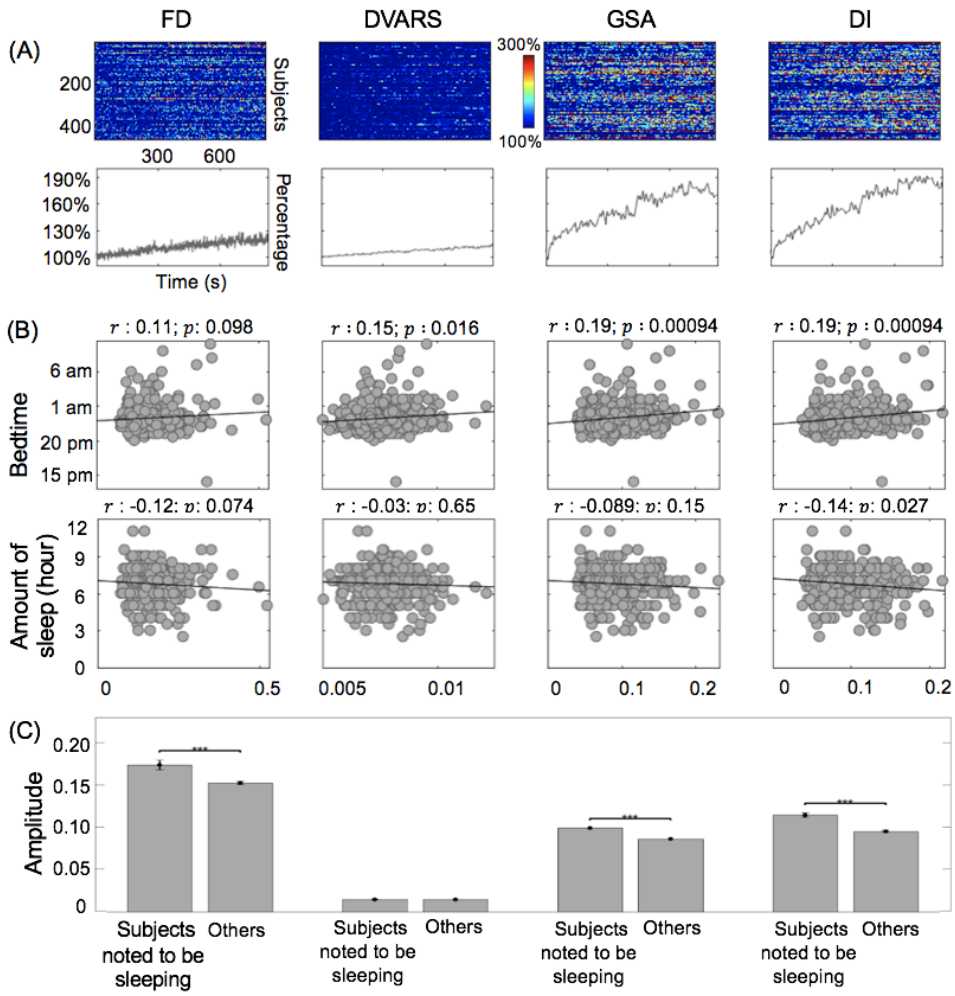

Figure 2 Motion and arousal metrics are related to brain arousal. (A) The amplitude of FD, DVARS, GSA, and DI increases over the course of resting-state scanning. Time courses of the four metrics, which were normalized with respect to their initial values during the first 14.4 seconds (20 TRs), are shown for each of 469 subjects (top panels), as well as their averages (bottom panels). (B) Cross-subject correlations between the mean FD, DVARS, GSA, and DI scores and two PSQI items, i.e., Bedtime and Amount of Sleep. Significant correlations were found between these two arousal-related behavioral measures and the DI scores, with Pearson's correlation coefficients and corresponding *p*-values (FDR corrected) being shown on the top. (C) 114 subjects, who were noted to be sleeping during the resting-state scanning sessions, show significantly higher DI score compared with the other subjects who were not. The error bar represents the standard error of the mean (SEM). The asterisks represent the level of significance: ***, $p < 0.001$.

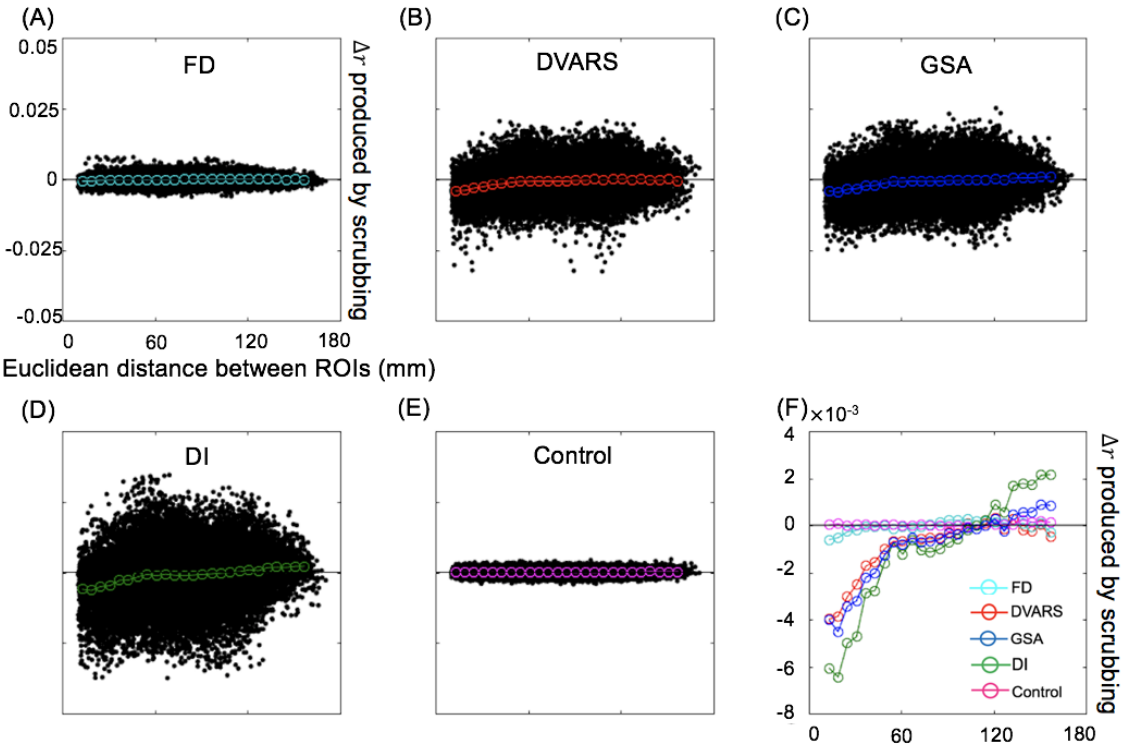

Figure 3 Effects of temporal scrubbing on resting-state fMRI connectivity. Removing time points with the top 25% values in FD (A), DAVRS (B), GSA (C), and DI (D) reduced the local but increased the long-range rsfMRI correlations between the 264 pre-defined brain ROIs, whereas temporal scrubbing using a control mask, which is created by circularly shifting the FD mask by 600 time points, produced no effects on rsfMRI connectivity (E). A comparison of temporal scrubbing based on different metrics (F) suggests that the DI-based scrubbing has the largest effect on rsfMRI connectivity.

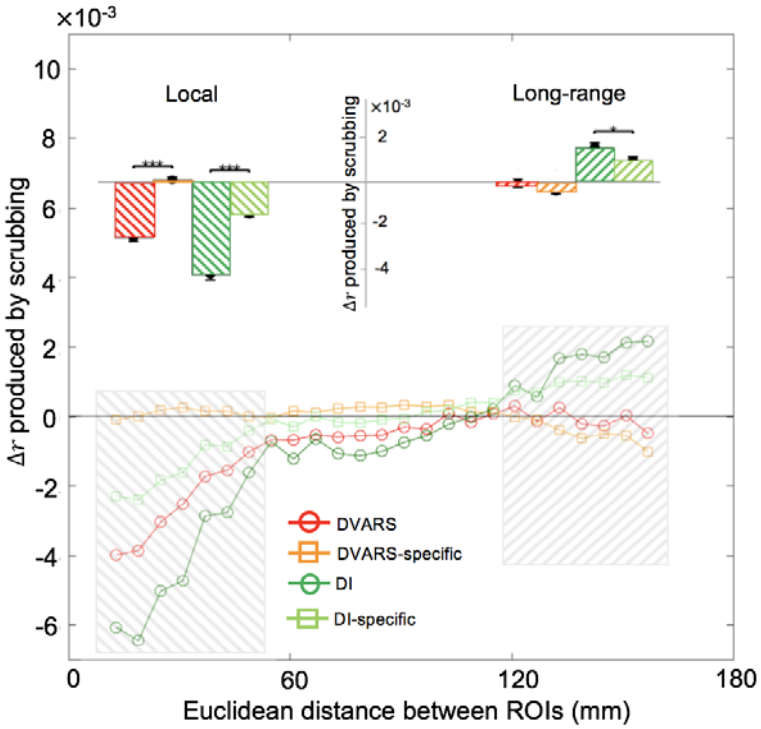

Figure 4 The effect of the DVARS-based scrubbing on rsfMRI connectivity diminished with retaining the high DI volumes. After removing the overlapped time points (9.81% out of 25%) between the DVARS and DI masks from temporal scrubbing, i.e., retaining them for assessing rsfMRI connectivity, the DVARS-specific scrubbing (orange square) produced no effects on the local and long-range rsfMRI connectivity. In contrast, the effect of the DI-specific scrubbing (light green square) remains significant. The local (ROI pairs with a distance between 13 and 49 mm) and long-range (ROI pairs with a distance between 125 and 161 mm) rsfMRI connectivity changes are summarized as a bar plot and shown as an inset in the top region. The error bar represents SEM across subjects. The asterisks represent the level of significance: *, $0.01 < p < 0.05$, and ***, $p < 0.001$.

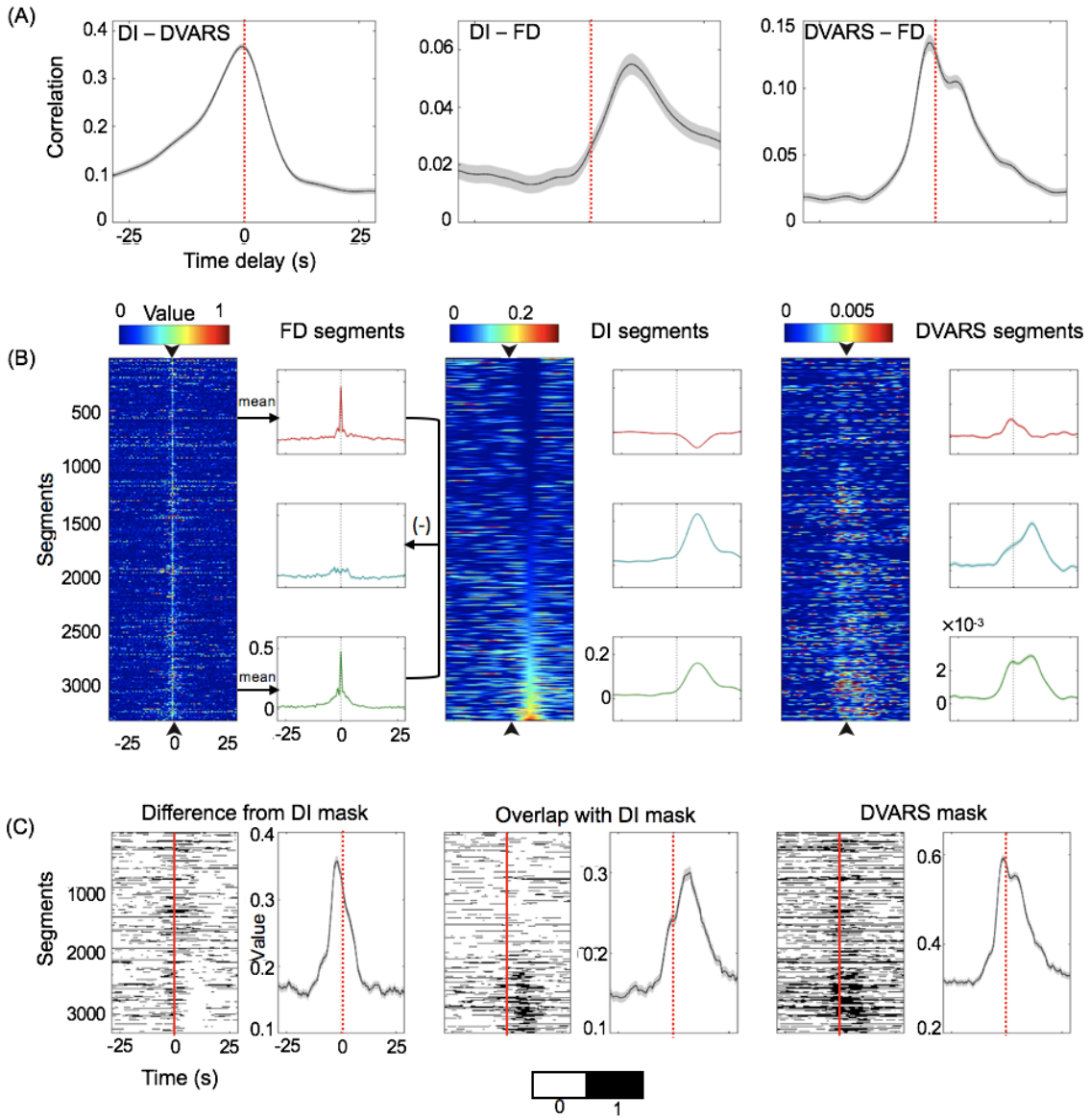

Figure 5 Temporal relationships among FD, DVARS and DI. (A) Cross-correlation functions of FD, DVARS, and DI. A zero-lag peak appears at the DI-DVARS correlation function (left); the maximum correlation between FD and DI appears with a ~9 seconds delay (middle); and the DVARS-FD correlation function shows two distinct peaks (right). The cross-correlation functions are averaged across subjects with the shaded region representing area within 1 SEM. (B) Segments of FD (left), DI (middle), and DVARS (right) were extracted with respect to the 3331 identified FD spikes (time 0) and sorted according to the DI values at 9.36 seconds. The top (red) and bottom (green) 400 segments were averaged and their differences (cyan) were also calculated. The shadow represents regions within one SEM. The black arrows indicate time zero. (C) Corresponding segments of the DVARS-based mask (right), its overlap with (middle) and difference from (left) the DI-based mask were also extracted and shown. The average of these segments is also shown on the right side of each panel with the shadow representing regions within one SEM.

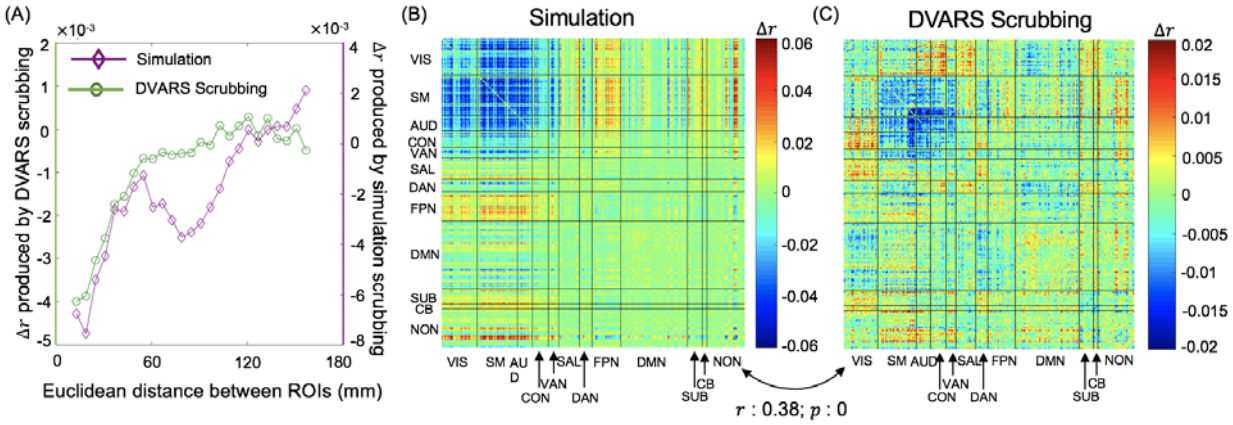

Figure 6 The global fMRI co-activation results in systematic rsfMRI connectivity changes. (A) Scrubbing simulated rsfMRI data with the global co-activation pattern (purple) reduced the local but increased the long-range rsfMRI correlations, similar to the DVARS-based temporal scrubbing (green). Expanding these 1D profiles into 2D matrices of inter-regional connectivity modulations further highlights the similarity between the two (B: Scrubbing simulated data; C: DVARS-based temporal scrubbing): the connectivity reductions are mainly within the sensory networks whereas the increase of connectivity are largely cross networks. The spatial correlation between (B) and (C) was 0.38 with $p = 0$. Resting-state network abbreviations: VIS: visual network; SM: somatomotor; AUD: auditory network; CON: cingulo-opercular; VAN: ventral attention; SAL: salience network; DAN: dorsal attention; FPN: fronto-parietal; DMN: default mode network; SUB: subcortical; CB: cerebellar; NON: uncertain network.

Tables

Table 1. Correlation of alert-related behavioral measures with FD, DVARS, GSA and DI

Behavioral measures	FD		DVARS		GSA		DI	
	Pearson r	p values	Pearson r	p values	Pearson r	p values	Pearson r	p valuess
PSQI_Score	0.14	0.027	0.060	0.30	0.045	0.47	0.063	0.30
Bed time	0.11	0.098	0.15	0.016	0.19	0.00094	0.19	0.00094
Amount of sleep	-0.12	0.074	-0.030	0.65	-0.089	0.15	-0.14	0.027
Minutes to fall asleep	0.080	0.22	0.0092	0.89	0.10	0.11	0.12	0.067
Get up time	0.020	0.70	0.093	0.14	0.12	0.07	0.093	0.14
Cannot get to sleep within 30 minutes	0.12	0.070	0.055	0.36	0.062	0.31	0.073	0.25
Wake up during sleep	0.11	0.081	-0.0045	0.93	-0.0083	0.89	0.023	0.73
Get up to use bathroom	0.070	0.28	-0.031	0.64	-0.031	0.64	-0.047	0.45
Breathe uncomfortably	0.16	0.0070	0.097	0.12	0.062	0.31	0.090	0.15
Snore loudly	0.23	0.000030	0.17	0.0031	0.014	0.84	0.049	0.43
Feel too cold	0.10	0.11	0.070	0.26	0.015	0.83	0.046	0.46
Feel too hot	0.14	0.027	0.044	0.48	-0.10	0.11	-0.056	0.35
Have bad dream	0.078	0.23	0.0087	0.89	0.068	0.27	0.072	0.25
Have pain	0.077	0.23	0.076	0.24	-0.061	0.31	-0.043	0.49
Other sleep troubles	-0.0050	0.93	-0.072	0.25	-0.097	0.12	-0.11	0.10
Overall sleep quality	0.075	0.25	0.0042	0.93	0.057	0.35	0.10	0.11
How often taken sleep medicine	-0.041	0.51	0.016	0.83	-0.039	0.53	-0.067	0.28
Trouble staying awake	0.10	0.11	0.061	0.31	0.078	0.23	0.095	0.13
Trouble keeping up enthusiasm	0.074	0.25	0.072	0.25	-0.029	0.65	0.0098	0.89
Have bed partner or roommate	-0.042	0.50	-0.11	0.089	-0.095	0.13	-0.070	0.26